

Testing anisotropic Hubble expansion

Paula Boubel,^a Matthew Colless,^a Khaled Said,^{b,c} and Lister Staveley-Smith^d

^aResearch School of Astronomy and Astrophysics, The Australian National University, Mount Stromlo Observatory, Canberra, ACT 2611, Australia

^bSchool of Mathematics and Physics, University of Queensland, Brisbane, QLD 4072, Australia

^cOzGrav: The ARC Centre of Excellence for Gravitational Wave Discovery, Hawthorn, VIC 3122, Australia

^dInternational Centre for Radio Astronomy Research (ICRAR), University of Western Australia, 35 Stirling Hwy, Crawley, WA 6009, Australia

E-mail: paula.boubel@anu.edu.au

Abstract. The cosmological principle asserting the large-scale uniformity of the Universe is a testable assumption of the standard cosmological model. We explore the constraints on anisotropic expansion provided by measuring directional variation in the Hubble constant, H_0 , derived from differential zeropoint measurements of the Tully-Fisher distance estimator. We fit various models for directional variation in H_0 using the Tully-Fisher dataset from the all-sky *Cosmicflows-4* catalog. The best-fit dipole variation has an amplitude of 0.063 ± 0.016 mag in the direction $(\ell, b) = (142 \pm 30^\circ, 52 \pm 10^\circ)$. If this were due to anisotropic expansion it would imply a 3% variation in H_0 , corresponding to $\Delta H_0 = 2.10 \pm 0.53$ km s⁻¹ Mpc⁻¹ if $H_0 = 70$ km s⁻¹ Mpc⁻¹, with a significance of 3.9σ . A model that includes this H_0 dipole is only weakly favored relative to a model with a constant H_0 and a bulk motion of the volume sampled by *Cosmicflows-4* that is consistent with the standard Λ CDM cosmology. However, we show that with the expected Tully-Fisher data from the WALLABY and DESI surveys it should be possible to detect a 1% H_0 dipole anisotropy at 5.8σ confidence and to distinguish it from the typical bulk flow predicted by Λ CDM over the volume of these surveys.

Contents

1	Motivation	1
2	Data	2
2.1	HI line widths	3
2.2	Photometry	3
3	Method	4
4	Results	6
4.1	H_0 dipole and quadrupole	6
4.2	Comparison with a bulk flow model	6
4.3	Pixel map of anisotropies	9
5	Simulations	11
5.1	Bulk flow versus H_0 dipole	11
5.2	Forecasts for future datasets	13
6	Conclusions	14

1 Motivation

The cosmological principle, the assumed isotropy and homogeneity of the universe on sufficiently large scales, has been put under increasing scrutiny over the past decade. Detections of an anisotropic expansion rate would create tension with this fundamental assumption of the standard model of cosmology. Hints of anisotropic expansion have been found in the quasar data [1–3] and Type Ia supernovae data [4–9].

Ref. [9] found that while the amplitude of the anisotropy is not statistically unlikely, its alignment with the CMB dipole is troubling, since these supernovae compilations have already been put in the CMB frame by construction. Ref. [8] found that the direction of the H_0 dipole differed from that of the CMB dipole by 3σ until a sufficiently high redshift cut was made, indicating that peculiar velocities corrections may be extremely important in H_0 determinations. Ref. [7] found a positive H_0 variation of order $1 \text{ km s}^{-1} \text{ Mpc}^{-1}$ in the direction of the CMB dipole, for both low- and high-redshift samples. Ref. [6] also found higher values of H_0 in the direction of the CMB dipole at $2\text{--}3\sigma$ significance. Most recently, refs. [4, 5, 10] examined the catalog of *Pantheon+* Type Ia supernovae [11] in the CMB frame and found a dipole anisotropy H_0 of $+2\text{--}4 \text{ km s}^{-1} \text{ Mpc}^{-1}$ in roughly the same direction as the CMB dipole. These studies hint at either a calibration problem or a possible misinterpretation of the CMB dipole in modern cosmology.

A study using galaxy scaling relations [12] found an anisotropy with a dipolar form corresponding to a 9% spatial variation of H_0 in the direction $(\ell, b) = (280 \pm 35^\circ, -15 \pm 20^\circ)$ or to a bulk flow of 900 km s^{-1} . This direction refers to a *lower* H_0 value compared to the rest of the sky. Using simulations, they determined that the significance of this was greater than 5σ . However, they stated that the effect of a H_0 dipole is inseparable from a bulk flow in their sample due to the low median redshift ($z = 0.1$). Still, the large bulk flow required would be in tension with assumptions in standard Λ CDM cosmology.

Subsequently, a similar analysis was performed by [13] while searching for systematic biases that could explain the previous result. They found no systematics large enough and their results were consistent with [12], finding a variation in the direction $(\ell, b) = (295 \pm 71^\circ, -30 \pm 71^\circ)$ with a significance of 3.6σ . Both of these studies present strong evidence for an anisotropy of galaxy scaling relations, but the underlying cause could be either an anisotropic H_0 or a large-scale bulk flow.

Theoretical frameworks for anisotropic expansions arising from arbitrary space-time metrics beyond the standard FLRW assumption have been studied. For example, [14] presents a model-independent multipole expansion of cosmological luminosity distances. Using simulations of this physical framework, the parameter that appears in place of the FLRW Hubble parameter was found to be dominated by a quadrupole [15, 16]. The maximum quadrupole found by [16] is typically 2% but can be as high as 5%, while [15] found a quadrupole strength of 0.565% on average for 100 observers. These results depend on the smoothing scale of the simulations. Using the *Pantheon+* catalog [11] to constrain this quadrupole in the Hubble parameter, [15] found a 1.96σ quadrupole even with velocity corrections.

In this study, we will use the Tully-Fisher relation to investigate this recurring theme and discover whether it is possible to disentangle the effect of bulk flows from a true H_0 anisotropy. As with the Type Ia supernovae studies, but *in contrast to* the galaxy scaling relation studies, we define the ‘direction’ of the H_0 dipole to be that of its maximum value.

The advantage of probing H_0 anisotropy, as opposed to the isotropic value of H_0 , is that differential measurements are not subject to systematics in the absolute calibration of H_0 . In fact, the presence of a H_0 anisotropy in the local Universe could have significant implications in the form of bias or additional sample variance for H_0 measurements that do not account for this possibility, since when isotropy is assumed, sky coverage is not typically considered in determinations of H_0 .

Although the use of the Tully-Fisher relation suffers from significant systematic errors in the determination of a H_0 monopole [17], its ability to detect H_0 variations is limited only by the statistical precision of the Tully-Fisher zeropoint. At present we may not have the precision required to adequately constrain anisotropic Hubble expansions, but the bounty of new Tully-Fisher data in the next few years may make useful constraints possible in the near future.

In Section 2 we describe the data used for this analysis; in Section 3 we describe the model used to constrain the anisotropies and its integration into our Bayesian methodology; in Section 4 we present the results for the anisotropies detected and their statistical significance compared to other models; in Section 5 we investigate our ability to distinguish anisotropic H_0 and bulk flows for current and future Tully-Fisher datasets; finally, in Section 6 we present the conclusions of this work.

2 Data

The *Cosmicflows-4* (CF4) catalog [21] is currently the largest full-sky catalog of galaxies with Tully-Fisher distances and peculiar velocities. It is derived from heterogeneous datasets and contains 10,737 galaxies with HI redshifts and line widths, together with optical or infrared photometry. Because the method of this paper relies on the identification of physical differences in the Tully-Fisher relationship in different regions of the sky, it is highly sensitive to systematic differences between sources of photometry or HI line widths. We therefore want the data to be as uniform as possible.

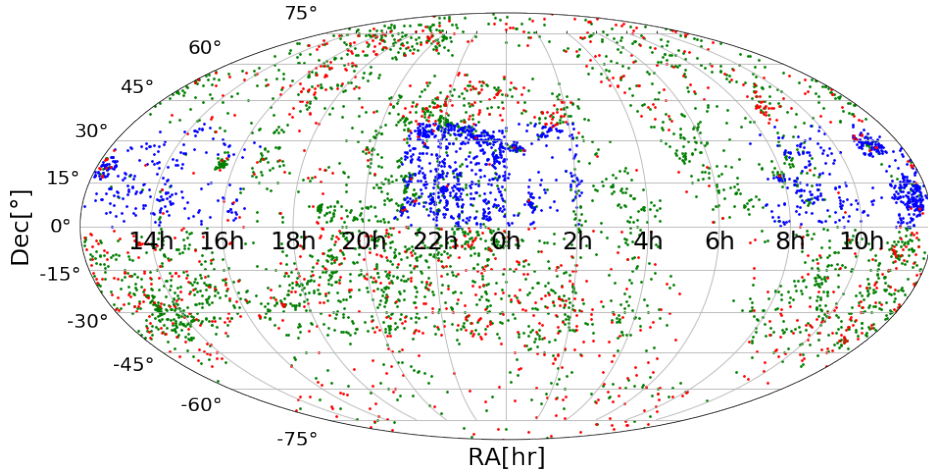


Figure 1: Sky distribution of HI sources with WISE magnitudes from the CF4 Tully-Fisher catalog. In blue, 1424 HI line-width measurements from ALFALFA [18]; in green, 2979 non-ALFALFA HI line-width measurements from the ADHI catalog [19]; in red, 1076 other sources from the *Springob/Cornell HI catalog* [20] or the *Pre Digital HI catalog* in EDD.

2.1 HI line widths

The data HI are taken primarily from the *All Digital HI (ADHI) catalog* [19], which is mainly composed of good quality HI line widths from the ALFALFA survey [18]. Sources not covered by the ALFALFA survey have HI line widths from the *Springob/Cornell HI catalog* [20] or the *Pre Digital HI catalog* on EDD¹, both containing measurements from a variety of large single-dish radio telescopes. The sky distributions of these various sources of HI line widths are shown in Figure 1. Even though the WISE data are all-sky, the 1424 sources covered by ALFALFA are all in the northern sky. To check for any systematic differences in HI line widths, in Figure 2 we compare the distributions of line widths from ALFALFA, from measurements in the northern sky, and measurements in the southern sky. When comparing the northern sky with the southern sky, a two-sample Kolmogorov–Smirnov (KS) test gives us a test statistic of 0.034 with a p -value of 0.077, so there is not enough confidence to say that the distributions are different. The median values and standard deviations of the distributions are $\log W_{\text{mx}}^c = 2.45 \pm 0.18$ in the north and $\log W_{\text{mx}}^c = 2.46 \pm 0.17$ in the south, so there is no reason to suspect a systematic difference between them.

2.2 Photometry

Although i -band optical photometry from the *Sloan Digital Sky Survey* [SDSS; 22] is available for 7502 CF4 galaxies in the northern sky, we choose to use $W1$ -band infrared photometry from the all-sky *Wide-field Infrared Satellite Explorer* [WISE; 23], available for 5479 CF4 galaxies, as using a single source of photometry over the whole sky mitigates against systematic variations.

¹<http://edd.ifa.hawaii.edu>; ‘Pre Digital HI’

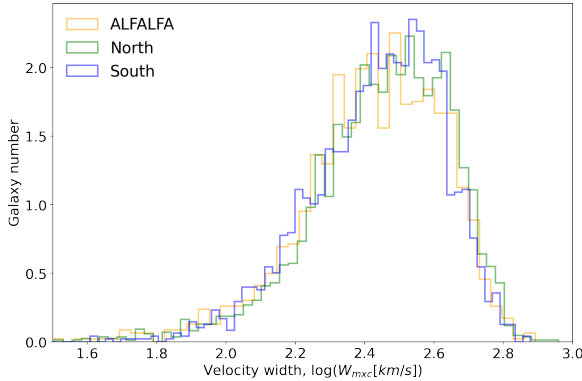


Figure 2: Normalized distributions of HI velocity widths from the CF4 Tully-Fisher catalog for all sources with $W1$ magnitude measurements from WISE. The distribution for sources in the northern sky are shown in green, sources in the southern sky in blue, and sources with line-width measurements from ALFALFA in orange.

3 Method

We have developed a forward-modeling methodology for simultaneously fitting the Tully-Fisher relation and peculiar velocity field in a sample of galaxies and applied it to the CF4 Tully-Fisher data [24] (see also [25]). The method formulates the conditional probability of observing an apparent magnitude m for a galaxy as

$$P(m | w, z, \alpha, \delta, \theta_{\text{TF}}, \theta_{\text{PV}}) = \frac{F(m) \exp \left[-\frac{(m-m')^2}{2\sigma_{\text{TF}}^2} \right]}{\int F(m) \exp \left[-\frac{(m-m')^2}{2\sigma_{\text{TF}}^2} \right] dm} \quad (3.1)$$

where m' is the predicted apparent magnitude as a function of the observed quantities HI velocity width w , redshift z , and position (α, δ) , and the parameters of the models for the Tully-Fisher relation θ_{TF} and the peculiar velocity field θ_{PV} ,

$$m'(w, z, \alpha, \delta, \theta_{\text{PV}}, \theta_{\text{TF}}) = M'(w) + 25 + 5 \log(1+z) + 5 \log d_C(z'_c) . \quad (3.2)$$

This predicted apparent magnitude is given in terms of $M'(w)$, the predicted absolute magnitude from the Tully-Fisher relation model for the observed HI velocity width $w \equiv \log W_{\text{mx}}^c - 2.5$, and z'_c , the predicted co-moving redshift from the peculiar velocity model for the observed redshift and position.

The zeropoint of the Tully-Fisher relation and the value of $h = H_0/100$ are directly related [17]; specifically, a shift in $5 \log h$ corresponds to a shift in M given by

$$M(w, h) = M(w, h = 1) + 5 \log h . \quad (3.3)$$

Consequently, it is not possible to use the Tully-Fisher relation on its own to determine H_0 . However, it is in principle possible to detect variations in H_0 using the *differential* Tully-Fisher relation, since changes in H_0 would be reflected by shifts in the Tully-Fisher zeropoint. This application does not rely on primary distance calibrations, but it does require high confidence in the spatial uniformity of the Tully-Fisher measurements, with negligible position-related systematic errors in the data.

Eq. 3.3 implies that a positive shift in $M(w)$, i.e. shifting the Tully-Fisher relation towards fainter magnitudes, corresponds to a positive shift in h . This can be understood intuitively – fainter predicted absolute magnitudes necessitate closer inferred distances if the apparent magnitude is held fixed, and so a larger H_0 is inferred for a fixed observed redshift. As a result, a positive Tully-Fisher zeropoint anisotropy corresponds to a positive H_0 anisotropy.

This paper explores the extent to which it is possible to measure H_0 anisotropies using the Tully-Fisher relation using current and future datasets.

We can model a direction-dependent H_0 by allowing the differential Tully-Fisher zeropoint to vary across the sky. In this scenario, the Tully-Fisher model [24] for the absolute magnitude given the velocity width, $M'(w)$, would have the form

$$M = \begin{cases} a_0(\ell, b) + a_1 w & (w < 0) \\ a_0(\ell, b) + a_1 w + a_2 w^2 & (w \geq 0) \end{cases} \quad (3.4)$$

where we have allowed a_0 to be a function of position on the sky, specified by ℓ (Galactic longitude) and b (Galactic latitude). Representing the variation on the sky in terms of a series expansion, we can fit the lowest-order spherical multipoles. The monopole and dipole terms can be described using four parameters ($a_{00}, a_{0x}, a_{0y}, a_{0z}$) as

$$a_0(\ell, b) = a_{00} + \tilde{a}_0(\ell, b) = a_{00} + a_{0x} \cos(b) \cos(\ell) - a_{0y} \cos(b) \sin(\ell) + a_{0z} \sin(b) \quad (3.5)$$

where the components of the dipole (a_{0x}, a_{0y}, a_{0z}) are represented in Cartesian coordinates in the Galactic reference frame in order to have Gaussian-distributed parameters.

In this work, the anisotropy model will be denoted $\tilde{a}_0(\ell, b)$ and will either be truncated at the dipole term, as above, or the quadrupole term, adding 5 more free parameters. Because the redshift range of the CF4 data is very limited, there is no need to include a decay factor as a function of redshift [15, 16], although this may be a consideration for future studies with more extensive datasets.

Assuming that the intrinsic Tully-Fisher relation is the same everywhere and that there are no differences in photometric calibration between different regions of the sky, variations in a_0 on the sky are due to variations in H_0 (parametrised as $h = H_0/100 \text{ km s}^{-1} \text{ Mpc}^{-1}$). The deviation of the measured Tully-Fisher zeropoint from its true value is

$$M(w, h(\alpha, \delta)) - M(w, \bar{h}) = \tilde{a}_0 = 5 \log h(\alpha, \delta) - 5 \log \bar{h} = 5 \log(\Delta h(\alpha, \delta)/\bar{h} + 1), \quad (3.6)$$

where \bar{h} is the mean value of h . This leads to

$$\Delta H_0 = \overline{H_0}(10^{\tilde{a}_0/5} - 1), \quad (3.7)$$

where we have replaced h with H_0 . Thus, differences in H_0 on the sky can be directly linked to the anisotropy of the Tully-Fisher zeropoint, \tilde{a}_0 .

In general, the Tully-Fisher parameters $a_0, a_1, a_2, \epsilon_0$, and ϵ_1 (see [24]) are unique to the dataset, as the Tully-Fisher relation changes depending on the photometric band. However, any real H_0 anisotropy should result in a consistent \tilde{a}_0 across datasets. We can therefore, in principle, combine datasets to achieve greater precision on constraints for the multipole terms of \tilde{a}_0 , whilst allowing the other Tully-Fisher parameters to vary. This only works if there are no spatial non-uniformities within individual photometric datasets.

4 Results

In this work, we use the *W1*-band Tully-Fisher data from CF4 because it provides uniform all-sky photometry. We apply a lower redshift limit, requiring $cz > 3000 \text{ km s}^{-1}$, as the large relative effects of peculiar velocities at low redshifts may have a significant impact on H_0 determinations. This is the same limit as was chosen in [17] to produce a H_0 that did not vary with redshift. Higher redshift limits reduced the size of the sample while only resulting in small changes ($< 1\sigma$) to the amplitude of the dipole; lower redshift limits slightly increased the significance of the dipole amplitude. Because a lower redshift limit greater than or equal to 3000 km s^{-1} produced consistent results, this value was chosen to preserve sample size while minimizing the effects of peculiar velocities.

4.1 H_0 dipole and quadrupole

Figure 3 shows the pairwise constraints, with contours at the 68% and 95% confidence levels, from fitting an a_0 monopole, dipole, and quadrupole to the CF4 *W1*-band data. The dipole is measured to have a significance of 3.9σ . Figure 4 is a visualization of these a_0 anisotropies on the sky, converting a_0 to the corresponding ΔH_0 assuming $H_0 = 70 \text{ km s}^{-1} \text{ Mpc}^{-1}$. The top panel of Figure 3 shows the fitted dipole, amplitude $\Delta H_0 = 2.10 \pm 0.53 \text{ km s}^{-1} \text{ Mpc}^{-1}$ in the direction $(\ell, b) = (142 \pm 30^\circ, 52 \pm 10^\circ)$. The dipole direction is not aligned with the external bulk flow fitted from the same data [24] nor with the CMB dipole determined by *Planck* [26]. The dipole minimum, however, is consistent with the direction of the largest (negative) H_0 anisotropy found in studies using galaxy cluster scaling relations [12, 13]. This minimum occurs at the antipode, $(\ell, b) = (322 \pm 29^\circ, -52 \pm 12^\circ)$.

We also fit a combination of a dipole and a quadrupole; the quadrupole adds 5 free parameters to the model. The direction is not fixed, as it was in previous studies [4, 15]. The middle panel of Figure 4 shows the best-fitting quadrupole (only); it has an amplitude of $|\tilde{a}_0| = 0.09 \pm 0.08 \text{ mag}$ ($\Delta H_0 = 3.0 \pm 2.6 \text{ km s}^{-1} \text{ Mpc}^{-1}$ if $H_0 = 70 \text{ km s}^{-1} \text{ Mpc}^{-1}$). The significance of this quadrupole term is low, only 1.1σ . The bottom panel of the figure shows the combined best-fit dipole plus quadrupole model.

4.2 Comparison with a bulk flow model

The presence of a residual bulk flow in the sample could be misinterpreted as an anisotropy in a_0 , because galaxy peculiar velocities modify their observed redshifts and so affect the predicted absolute magnitudes. As with H_0 , the direction of the bulk flow is in the same direction as that of the a_0 dipole maximum. This can be understood by looking at the effect of a peculiar velocity v on the inferred cosmological redshift z_c at a fixed observed redshift z :

$$1 + z = (1 + z_c)(1 + v/c). \quad (4.1)$$

A higher, positive value for v reduces z_c , resulting in a smaller inferred distance (for a fixed H_0). A closer galaxy must therefore be intrinsically fainter, since its apparent magnitude is a fixed, observed quantity. This means that the Tully-Fisher zeropoint is shifted to more positive values.

However, a bulk flow is, in principle, distinguishable from a H_0 sky variation, mainly because the effect on a_0 of a bulk flow depends on a galaxy's redshift while the effect of a H_0 variation does not. As a result, a bulk flow will not create a pure spatial dipole in a_0 unless the redshift is fixed. Thus, redshift coverage and sky coverage are both important to being able to distinguish between them.

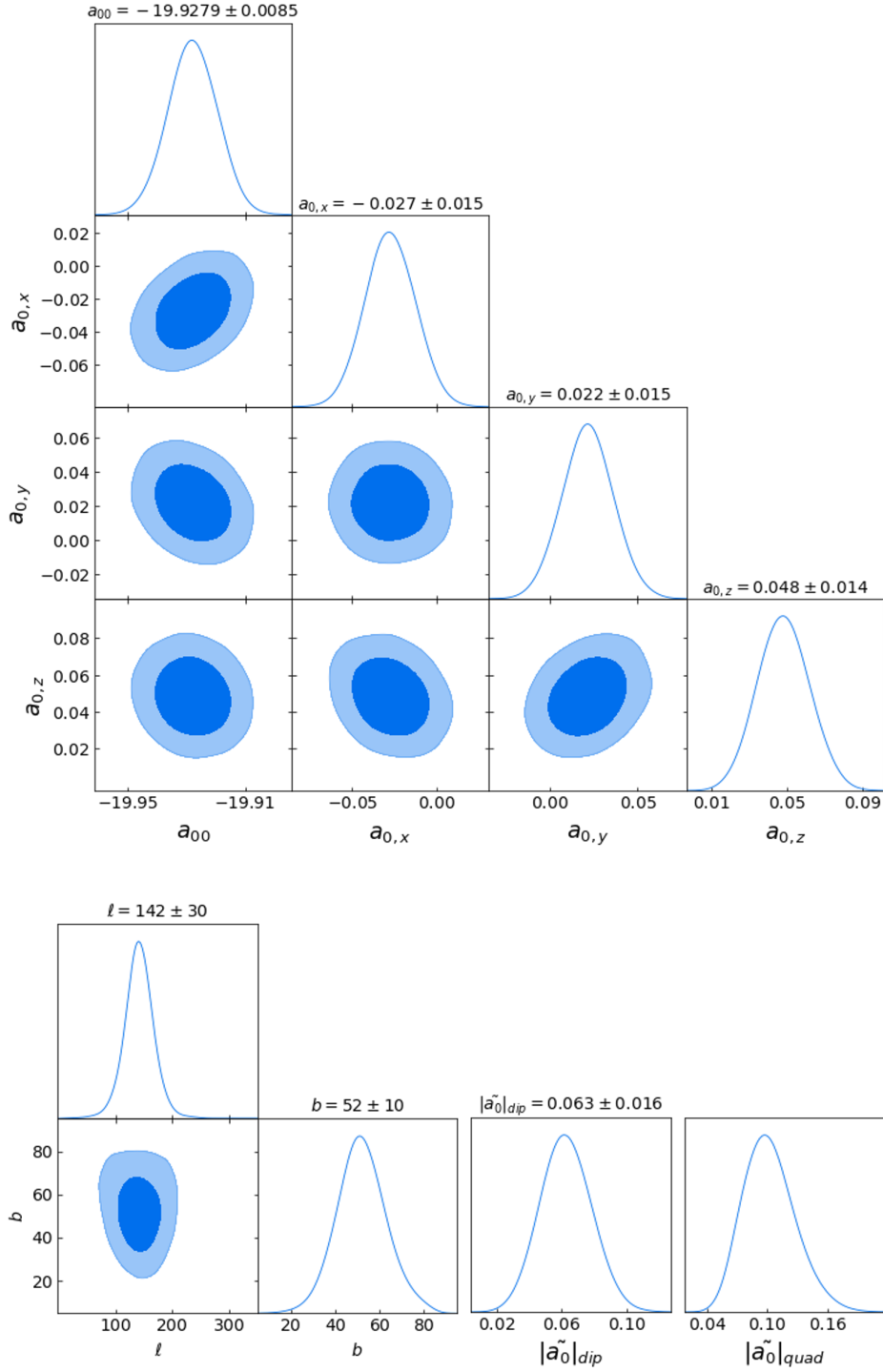


Figure 3: Constraints from fitting a Tully-Fisher zeropoint monopole, dipole, and quadrupole to the W1 CF4 data. Top cornerplot: best-fit monopole $a_{00} = -19.928 \pm 0.009$ mag and dipole $\tilde{a}_0 = (a_{0x}, a_{0y}, a_{0z}) = (-0.027 \pm 0.015, 0.022 \pm 0.015, 0.048 \pm 0.014)$ mag. Bottom cornerplot: dipole direction is $(l, b) = (142 \pm 30^\circ, 52 \pm 10^\circ)$ and amplitude is $|\tilde{a}_0|_{dip} = 0.063 \pm 0.016$ mag; best-fit quadrupole amplitude is $|\tilde{a}_0|_{quad} = 0.09 \pm 0.08$ mag.

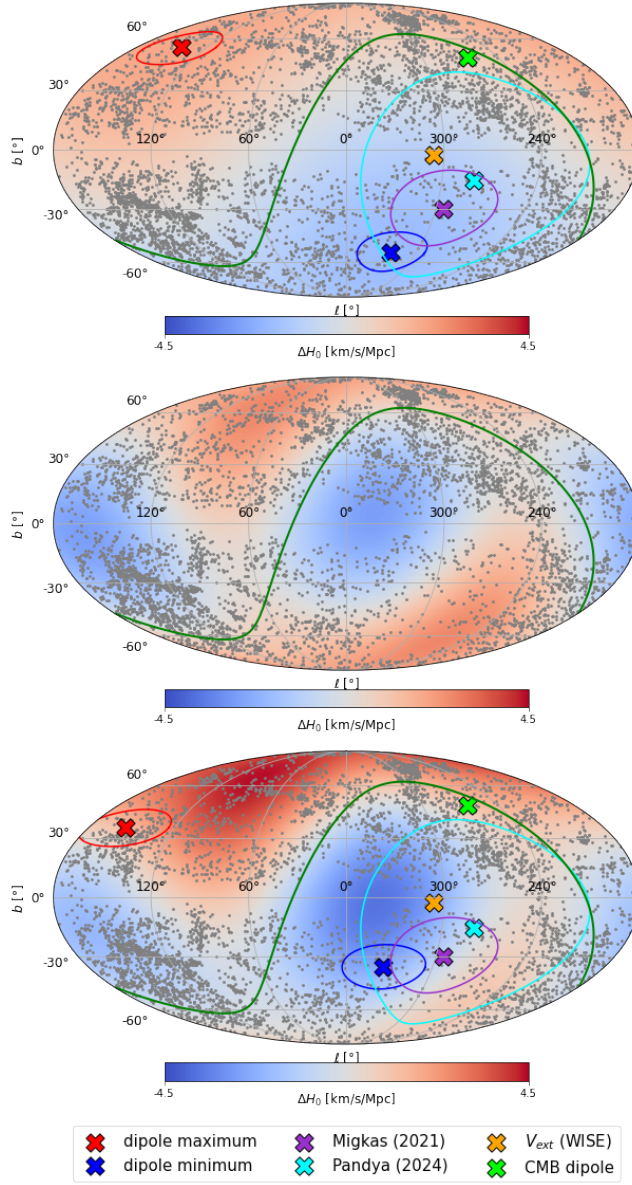


Figure 4: Mollweide projections of anisotropies in Galactic coordinates. Top: The best-fit H_0 dipole, where the direction of its $+/-$ value is shown by the red/blue crosses and the 1σ error boundary is shown by the red/blue ellipses. The amplitude is $\Delta H_0 = 2.10 \pm 0.53 \text{ km s}^{-1} \text{ Mpc}^{-1}$ if $H_0 = 70 \text{ km s}^{-1} \text{ Mpc}^{-1}$ and the direction of the maximum is $(\ell, b) = (142 \pm 30^\circ, 52 \pm 10^\circ)$. The gray points are the *W1*-band CF4 galaxies used in this fitting. The direction of the *Planck* CMB dipole [26] in the heliocentric frame is shown by the green cross. The direction of the external bulk flow from outside the 2M++ volume \mathbf{V}_{ext} (*W1*-band fit from [24]) is shown by the orange cross. The purple and light blue crosses and ellipses are directions of maximum H_0 anisotropy measured by [12, 13] using galaxy scaling relations. The green line traces out the celestial equator. Middle: Best-fit H_0 quadrupole with amplitude $\Delta H_0 = 3.0 \pm 2.6 \text{ km s}^{-1} \text{ Mpc}^{-1}$ if $H_0 = 70 \text{ km s}^{-1} \text{ Mpc}^{-1}$. Bottom: Sum of best-fit dipole and quadrupole.

M_0	M_1	$\ln(B_{01})$
velocity dipole	H_0 dipole	4.7
H_0 dipole	H_0 dipole and quadrupole	7.5
velocity and H_0 dipole	H_0 dipole	5.7
velocity dipole and H_0 dipole	velocity	0.99

Table 1: Bayes factors of fitting various models to the CF4 $W1$ Tully-Fisher data. In each scenario, M_0 is the preferred model with the lower BIC. The third column is the Bayes factor, $\ln(B_{01})$, and a higher value indicates stronger evidence for the preferred model.

For the currently available data, the CF4 Tully-Fisher catalog, we can fit a zeropoint dipole and quadrupole, as described in the previous sections, or we can instead fit a velocity dipole, or we can try to constrain both simultaneously. To compare the fits from these models, we can compute the Bayes factor

$$B_{01} \equiv \frac{P(d|M_0)}{P(d|M_1)} \quad (4.2)$$

where B_{01} is the posterior odds that model M_0 is true rather than model M_1 , in light of the data d and assuming equal priors for both models [27, 28]. In our case, the number of data points n is much greater than the number of parameters k , so we can use the following approximation:

$$P(d|M) \approx \exp\left(- (k \ln n - 2 \ln \hat{L})/2\right) \quad (4.3)$$

where \hat{L} is the maximum likelihood of the model M . The quantity $k \ln n - 2 \ln \hat{L}$ is the Bayesian information criterion, BIC [29]. A lower BIC is preferred, meaning that a model is penalized if it requires more parameters k . So,

$$\ln(B_{01}) \approx (\text{BIC}(M_1) - \text{BIC}(M_0))/2 . \quad (4.4)$$

Table 1 lists the Bayes factors for different model fits to the CF4 $W1$ Tully-Fisher data. Using the recommended interpretation of [30] (adapted from the original Jeffreys scale [31]), also used in other cosmological analyses (for example: refs. [32, 33]), we see strong evidence of a velocity dipole rather than a H_0 dipole if we had to choose between the two. Secondly, there is weak evidence that a velocity dipole with an additional H_0 dipole is favored over a velocity dipole only. Lastly, a H_0 dipole term alone is strongly favored over a model that incorporates both a dipole and a quadrupole, suggesting that the quadrupole term adds too many parameters with minimal improvement in fitting the data.

4.3 Pixel map of anisotropies

In the previous sections, we have fit for the dipole and quadrupole variation of H_0 on the sky. We lack sufficient data to extract any higher-order information with confidence (even fitting a quadrupole adds little or no value; see Table 1). However, we can get a rough picture of any smaller-scale anisotropies, if they exist, by binning the data on the sky and fitting a constant a_0 separately for each bin.

For this exercise, we choose the HEALPix [34] binning scheme with NSIDE=2, corresponding to 48 total pixels of equal area on the sky. Using the CF4 $W1$ data, we fit a

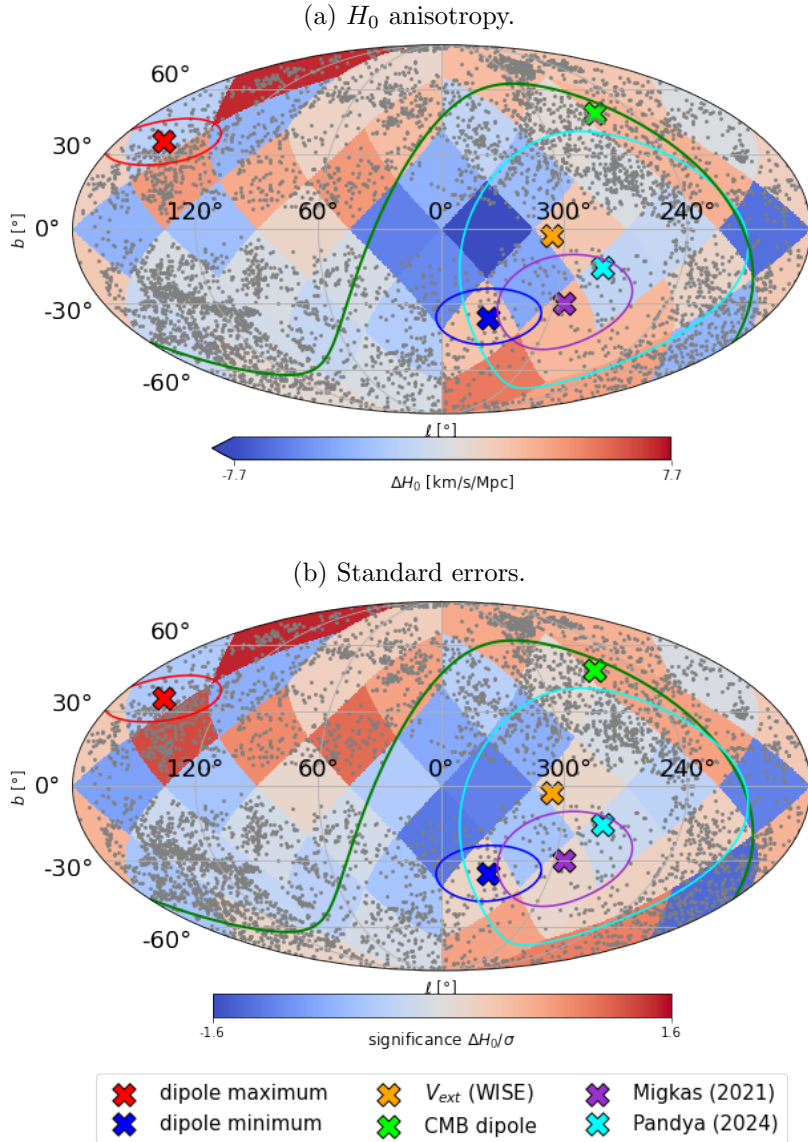


Figure 5: (a) Best-fit Tully-Fisher zeropoints for CF4 $W1$ data (gray points) binned in HEALPix pixels (resolution $\text{NSIDE}=2$), expressed as ΔH_0 using Equation (3.7). The red/blue crosses show the best-fit \pm dipole direction determined in Section 4.1. (b) Significance of the anisotropy in each pixel, as indicated by the best-fit values from the top panel divided by their standard errors.

different a_0 to the galaxies in each pixel, fixing all the other Tully-Fisher and peculiar velocity parameters to those obtained from fitting the full dataset. To find the mean, a_{00} , we take the average of the a_0 values weighted by uncertainty. Then, $a_0 - a_{00}$ gives the value of $\tilde{a}_0(\alpha, \delta)$ for that pixel. These values can be converted to ΔH_0 using Equation (3.7). The result is the map shown in Figure 5.

5 Simulations

In order to estimate the statistical uncertainties on the dipole measurement, \tilde{a}_0 , we will simulate mock CF4 datasets. The procedure for generating these mocks is detailed in Section 5 of [24]. Here we use the same procedure, with a few modifications made for each of the tests described below.

5.1 Bulk flow versus H_0 dipole

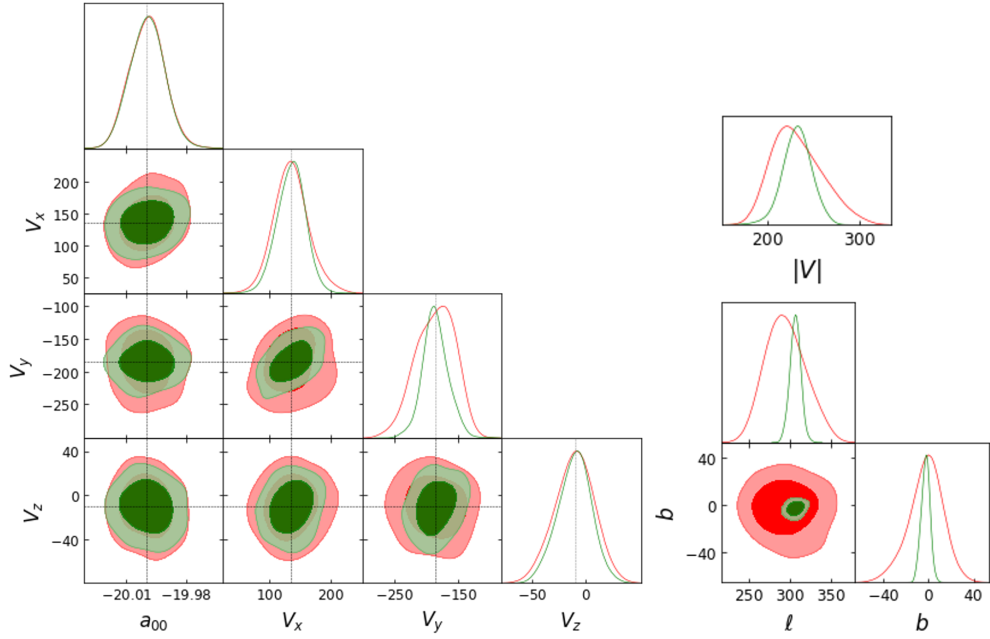
In the previous work [24], the external bulk flow was determined for the CF4 Tully-Fisher dataset separately for two bands i and $W1$. In Cartesian equatorial coordinates, the external velocity dipole in the $W1$ -band was found to be $\mathbf{V}_{\text{ext}} = (-90 \pm 10, +35 \pm 9, -209 \pm 9) \text{ km s}^{-1}$. If we assume a velocity dipole of this magnitude and direction is present in the data, we can show if and how it can be distinguished from a true a_0 (and corresponding H_0) dipole using CF4 mocks.

We use the procedure of [24] to create our mocks, but without peculiar velocities. We add a bulk flow of $\mathbf{V}_{\text{ext}} = (-90 \pm 10, +35 \pm 9, -209 \pm 9) \text{ km s}^{-1}$ to each galaxy, modifying its observed redshift and thus its apparent magnitude (see Eq. (3.2)). Fitting the Tully-Fisher relation and a bulk flow term to these mocks should faithfully recover all parameters. Alternatively, fitting a Tully-Fisher relation with a zeropoint dipole and no bulk flow term gives a model for a H_0 dipole that approximates the actual bulk flow.

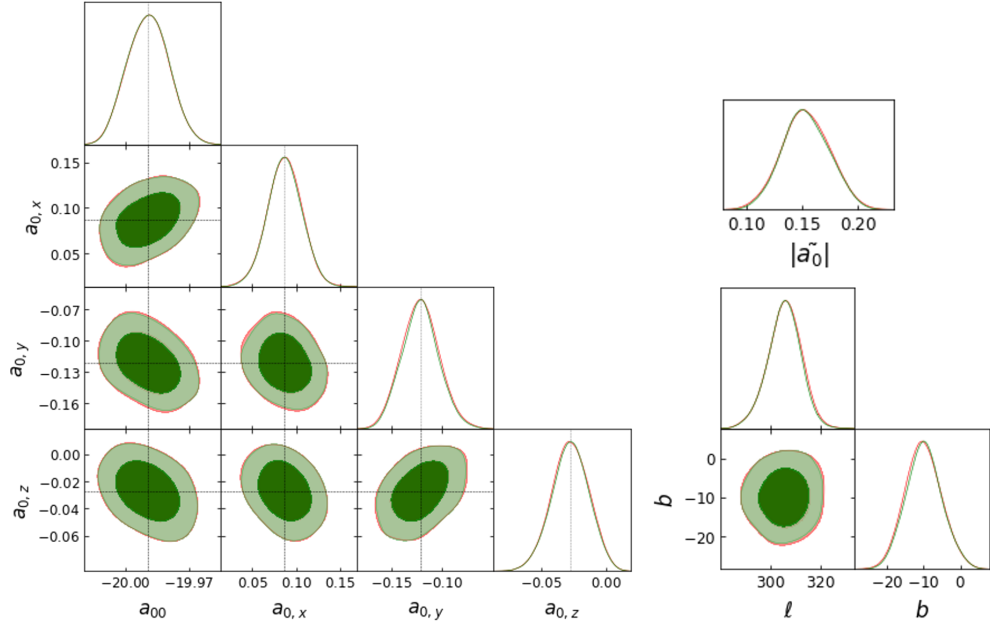
This model can then be used to generate a new suite of mocks with a zeropoint (H_0) dipole rather than a bulk flow. Again, we fit both a velocity dipole and a zeropoint dipole to this new set of mocks. This exercise provides insight into our ability to distinguish a H_0 dipole from a velocity dipole in the existing dataset. Figure 6 shows the resulting pairwise constraints on a_{00} , a_{0x} , a_{0y} , and a_{0z} for each of these four tests. Green contours represent cases where the fitted model matches the simulated model, while red contours represent fits of the incorrect model. The gray hashed lines show the input parameters of the simulations.

The power of the CF4 Tully-Fisher dataset to determine which is the correct dipole model is summarized in Figure 7a. This shows the distribution of Bayes factors favoring the correct model over the incorrect model in mock CF4 datasets. If there is an H_0 (i.e., a_0) dipole in the CF4 Tully-Fisher data, we would not be able to easily determine if we have the correct model or not, as the Bayes factor is relatively small (blue histogram; median $\ln(B_{01}) = 2$). However, if there is a velocity dipole (bulk flow) in the CF4 Tully-Fisher data, the Bayes factor would show significant evidence favoring the correct model (red histogram; median $\ln(B_{01}) = 79$).

There are two reasons for this: firstly, the median intrinsic scatter in the Tully-Fisher relation in CF4 data is at least 0.5 mag [24], corresponding to roughly a 25% error on H_0 that depends on distance, whereas the bulk flow has a much smaller error of $\pm 10 \text{ km s}^{-1}$ in each component [24], corresponding to a $\sim 0.1\%$ variation in H_0 that is distance-independent. Secondly, the direction we have chosen for the dipoles lies close to the Zone of Avoidance (the plane of the Milky Way), so the dipole is less constrained in the context of the sky distribution of our mock sample.



(a) Fitting a velocity bulk flow.



(b) Fitting a Tully-Fisher zeropoint dipole.

Figure 6: (a) Fitting a velocity dipole (V_x , V_y , V_z) in km s^{-1} to 1000 CF4 mocks. The mocks shown in green used a velocity dipole indicated by the gray lines; the mocks shown in red used an approximately corresponding H_0 dipole. (b) Fitting a H_0 dipole model (Eq.(3.5)) to 1000 CF4 mocks. The mocks shown in green used a H_0 dipole indicated by the gray lines; the mocks in red used an approximately corresponding velocity field dipole. In both panels, the 2D distributions are shown on the left for the Cartesian components and the same information is presented in spherical coordinates on the right: 1D distributions for the dipole amplitude of (a) \mathbf{V}_{ext} in km s^{-1} or (b) \tilde{a}_0 in mag, plus 2D distributions for the dipole direction in Galactic coordinates ℓ and b in degrees.

5.2 Forecasts for future datasets

CF4 is currently the largest collection of galaxies with Tully-Fisher data, but this is rapidly changing with upcoming HI surveys like the *Wide-field ASKAP L-band Legacy All-sky Blind survey* [WALLABY; 35, 36] and the *FAST All Sky HI Survey* [FASHI; 37, 38]. FASHI is expected to detect more than 100,000 HI sources covering more than 22,000 deg² between declinations -14° and +66° [37], and has already released HI measurements for over 40,000 sources [38]. WALLABY is expected to detect 210,000 HI sources over 14,000 deg² [36] of the southern sky by 2027. Both surveys have a redshift limit around $z \approx 0.1$. Not all HI sources can be used in fitting the Tully-Fisher relation, as the signal-to-noise ratio needs to be sufficiently high and the inclination sufficiently edge-on. In WALLABY, it is expected that about 40% of sources will meet these criteria [39]. In addition, the DESI peculiar velocity survey [DESI; 40] is expected to obtain stellar rotation velocities enabling about 50,000 Tully-Fisher peculiar velocity measurements over an area of 14,000 deg² of the northern sky within two years. These surveys should result in an order-of-magnitude increase in sample size relative to the CF4 Tully-Fisher catalog over the next few years. They will also reach higher redshifts (up to $z \approx 0.1$) and can be combined for greater sky coverage.

Anticipating this bounty of new data, we can repeat the above exercise with a mock dataset that reflects these improvements in sky coverage, redshift range, and sample size. For these mocks, we combine the expected redshift and sky distributions of the 50,000 targets selected for the DESI Tully-Fisher peculiar velocity survey [40] with 80,000 galaxy positions

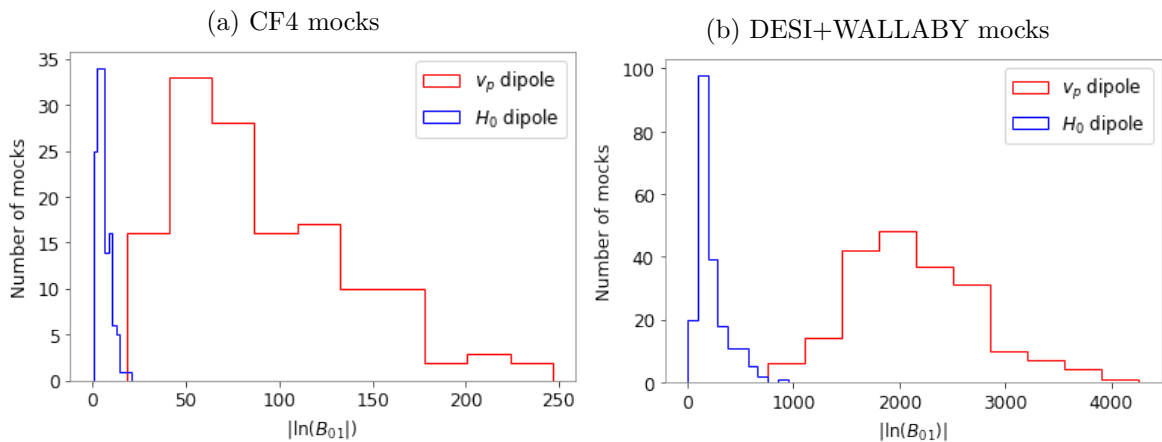


Figure 7: (a) The logarithm of the Bayes factor for the correct dipole model relative to the incorrect dipole model in 250 mock CF4 Tully-Fisher datasets. Blue: the true model is a H_0 (Tully-Fisher zeropoint) dipole and the median $\ln(B_{01}) = 2$, showing barely any evidence favoring the correct model M_0 . Red: the true model is a velocity dipole and the median $\ln(B_{01}) = 79$, showing strong evidence favoring the correct model. (b) Forecast of the logarithm of the Bayes factor for the correct dipole model relative to the incorrect dipole model in 250 mock DESI+WALLABY Tully-Fisher datasets. Blue: the intrinsic model is a H_0 (Tully-Fisher zeropoint) dipole and the median $\ln(B_{01}) = 172$, showing very strong evidence favoring the correct model M_0 . Red: the intrinsic model is a velocity dipole and the median $\ln(B_{01}) = 2090$, showing decisive evidence favoring the correct model.

and redshifts drawn from the WALLABY reference simulation [35]². Figure 8 shows how the redshift and sky distributions of these samples compare to the CF4 Tully-Fisher catalog (WALLABY in green, DESI in blue, CF4 in red). Mock Tully-Fisher data is generated for these mock galaxies using the procedure described in Section 5.2 of [24]. We perform the same tests on these mocks as for the CF4 mocks in the previous section. Again, we assume a 3% dipole anisotropy in H_0 or a velocity dipole with the amplitude of the external bulk flow measured by [41], both in the same direction as the external bulk flow.

As with the mocks in Section 5.1, we test our ability to distinguish a velocity dipole from a H_0 dipole on the WALLABY+DESI mocks. For a 3% H_0 dipole amplitude, the measured signal has a significance of 9σ when fitting for the H_0 dipole. Figure 7b compares the Bayes factors from the WALLABY+DESI mocks, which very strongly favor the correct model for the anisotropy (whether that is an H_0 dipole or a velocity dipole). Between the CF4 mocks and the WALLABY+DESI mocks, the $\ln B_{01}$ values increase by a factor of 25–85. This huge improvement implies that future data should be able to much more strongly constrain a H_0 dipole, even in the presence of a residual velocity dipole. Even if the strength of the H_0 dipole is reduced to only 1%, we find that WALLABY+DESI will be able to detect it with 5.8σ significance.

6 Conclusions

We have exploited the ability of the Tully-Fisher relation to test for direction-dependence of H_0 with relatively simple differential zeropoint measurements, resulting from the fact that only the zeropoint of the relation is affected by changes in H_0 . Using the best current Tully-Fisher data, the *Cosmicflows-4* catalog, we fit for the Tully-Fisher zeropoint while allowing for variation on the sky in the form of a dipole, a quadrupole (which has some physical motivation [14–16]), or both (Section 4.1).

The best-fit zeropoint dipole, \tilde{a}_0 , is $(a_{0x}, a_{0y}, a_{0z}) = (-0.027 \pm 0.015, 0.022 \pm 0.015, 0.048 \pm 0.014)$ mag with a direction in Galactic coordinates $(\ell, b) = (142 \pm 30^\circ, 52 \pm 10^\circ)$.

²The WALLABY reference simulation is based on the initial plans for the survey, so its footprint and redshift distribution are now out of date. The full simulation has been downsized appropriately to reflect the current expected Tully-Fisher sample.

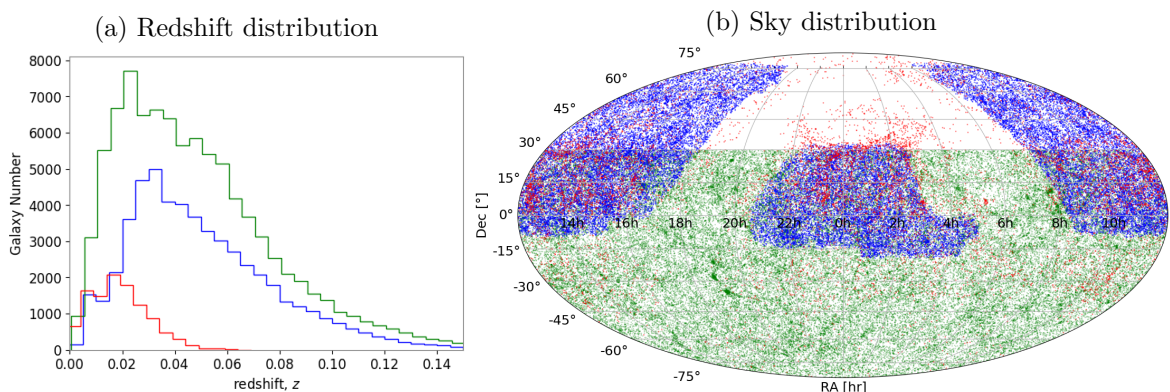


Figure 8: The expected (a) redshift and (b) sky distributions for the expected Tully-Fisher data from WALLABY (green) and DESI (blue) compared to existing CF4 data (red).

The dipole amplitude is $|\tilde{a}_0| = 0.063 \pm 0.016$ mag, implying $\Delta H_0 = 2.10 \pm 0.53$ km s⁻¹ Mpc⁻¹ if $H_0 = 70$ km s⁻¹ Mpc⁻¹, a 3% variation of H_0 . If real, this anisotropy would have important implications for the uncertainties in measurements H_0 and the Hubble tension.

The best-fit H_0 quadrupole has an amplitude $|\tilde{a}_0| = 0.09 \pm 0.08$ mag, corresponding to $\Delta H_0 = 3.0 \pm 2.6$ km s⁻¹ Mpc⁻¹ if $H_0 = 70$ km s⁻¹ Mpc⁻¹. This is not a statistically significant result. A Bayes factor of $\ln B_{01} = 7.5$ when comparing a dipole-only fit to a dipole+quadrupole fit strongly suggests that the improvement to the fit resulting from the quadrupole term is not justified by the additional parameters.

Assuming no systematic difference in the photometric calibration in different parts of the sky, the other physical effect that may cause anisotropies in a_0 is an unaccounted-for velocity dipole. This complicates our analysis because a large residual bulk flow is known to exist [24]. While the effect of a velocity dipole on a_0 is different to that of an H_0 dipole variation, the two may be difficult to distinguish with insufficient data. In this context, sample size, sky coverage, and redshift range are all important.

From the CF4 data, there is only weak evidence (Bayes factor $\ln B_{01} = 0.99$) that fitting a H_0 dipole in addition to a velocity dipole is favored to a velocity dipole only. This suggests that the existing data is insufficient to constrain a H_0 dipole and the apparent 3% variation of H_0 on the sky could plausibly be due to a residual bulk flow.

The direction of the dipole does not have any obvious physical significance. It is not aligned with the CMB dipole, so whatever is producing the dipole detected in previous SNIa studies is not present in this Tully-Fisher dataset. It is also not aligned with the Galactic or celestial poles (there is no sign of a north–south miscalibration). However, it is consistent with the direction of minimum anisotropy obtained from galaxy scaling relations [12, 13].

In order to generate forecasts for the potential of future datasets, we applied this method to mocks of the expected dataset from the combined WALLABY and DESI Tully-Fisher surveys. These much larger new datasets significantly tighten the constraints on a H_0 dipole relative to a velocity dipole. This anticipated expansion in sample size, redshift range and sky coverage increases the Bayes factor $\ln B_{01}$ by a factor of 25–85. This will be sufficient to detect a 1% H_0 dipole anisotropy with 5.8σ significance and to clearly distinguish it from a velocity dipole of similar amplitude.

Acknowledgments

MMC acknowledges support from a Royal Society Wolfson Visiting Fellowship at the University of Oxford (RSWVF\R3\223005). KS acknowledges support from the Australian Government through the Australian Research Council Centre of Excellence for Gravitational Wave Discovery (OzGrav) through project number CE230100016. We acknowledge use of the following analysis packages: Astropy [42], GetDist [43], emcee [44], and Matplotlib [45].

References

- [1] C. Krishnan, R. Mohayaee, E.O. Colgáin, M.M. Sheikh-Jabbari and L. Yin, *Does Hubble tension signal a breakdown in FLRW cosmology?*, *Classical and Quantum Gravity* **38** (2021) 184001.
- [2] N.J. Secrest, S. von Hausegger, M. Rameez, R. Mohayaee, S. Sarkar and J. Colin, *A test of the cosmological principle with quasars*, *ApJL* **908** (2021) L51.
- [3] N.J. Secrest, S. von Hausegger, M. Rameez, R. Mohayaee and S. Sarkar, *A challenge to the standard cosmological model*, *ApJL* **937** (2022) L31.

- [4] A. Sah, M. Rameez, S. Sarkar and C. Tsagas, *Anisotropy in Pantheon+ supernovae*, 2024.
- [5] R. Mc Conville and E. Ó Colgáin, *Anisotropic distance ladder in Pantheon+ supernovae*, *Phys. Rev. D* **108** (2023) 123533.
- [6] O. Luongo, M. Muccino, E.O. Colgáin, M.M. Sheikh-Jabbari and L. Yin, *Larger H_0 values in the CMB dipole direction*, *Phys. Rev. D* **105** (2022) 103510.
- [7] C. Krishnan, R. Mohayaee, E.O. Colgáin, M.M. Sheikh-Jabbari and L. Yin, *Hints of FLRW breakdown from supernovae*, *Phys. Rev. D* **105** (2022) 063514.
- [8] F. Sorrenti, R. Durrer and M. Kunz, *The dipole of the Pantheon+SH0ES data*, *JCAP* **2023** (2023) 054.
- [9] Z. Zhai and W.J. Percival, *Sample variance for supernovae distance measurements and the Hubble tension*, *Phys. Rev. D* **106** (2022) 103527.
- [10] Hu, J. P., Wang, Y. Y., Hu, J. and Wang, F. Y., *Testing the cosmological principle with the Pantheon+ sample and the region-fitting method*, *A&A* **681** (2024) A88.
- [11] D. Scolnic, D. Brout, A. Carr, A.G. Riess, T.M. Davis, A. Dwomoh et al., *The Pantheon+ analysis: The full data set and light-curve release*, *ApJ* **938** (2022) 113.
- [12] K. Migkas, F. Pacaud, G. Schellenberger, J. Erler, N.T. Nguyen-Dang, T.H. Reiprich et al., *Cosmological implications of the anisotropy of ten galaxy cluster scaling relations*, *A&A* **649** (2021) A151.
- [13] Pandya, A., Migkas, K., Reiprich, T. H., Stanford, A., Pacaud, F., Schellenberger, G. et al., *Examining the local Universe isotropy with galaxy cluster velocity dispersion scaling relations*, *A&A* **691** (2024) A355.
- [14] A. Heinesen, *Multipole decomposition of the general luminosity distance Hubble law — a new framework for observational cosmology*, *JCAP* **2021** (2021) 008.
- [15] J.A. Cowell, S. Dhawan and H.J. Macpherson, *Potential signature of a quadrupolar hubble expansion in Pantheon+ supernovae*, *MNRAS* **526** (2023) 1482.
- [16] H.J. Macpherson and A. Heinesen, *Luminosity distance and anisotropic sky-sampling at low redshifts: A numerical relativity study*, *Physical Review D* **104** (2021) .
- [17] P. Boubel, M. Colless, K. Said and L. Staveley-Smith, *An improved Tully–Fisher estimate of H_0* , *MNRAS* **533** (2024) 1550.
- [18] M.P. Haynes, R. Giovanelli, B.R. Kent, E.A.K. Adams, T.J. Balonek, D.W. Craig et al., *The Arecibo Legacy Fast ALFA Survey: The ALFALFA extragalactic H I source catalog*, *ApJ* **861** (2018) 49.
- [19] H.M. Courtois, R.B. Tully, J.R. Fisher, N. Bonhomme, M. Zavodny and A. Barnes, *The extragalactic distance database: All digital H I profile catalog*, *AJ* **138** (2009) 1938.
- [20] C.M. Springob, M.P. Haynes, R. Giovanelli and B.R. Kent, *A digital archive of H I 21 centimeter line spectra of optically targeted galaxies*, *ApJS* **160** (2005) 149.
- [21] E. Kourkchi, R.B. Tully, S. Eftekharzadeh, J. Llop, H.M. Courtois, D. Guinet et al., *Cosmicflows-4: The catalog of $\sim 10,000$ Tully–Fisher distances*, *ApJ* **902** (2020) 145.
- [22] D.G. York, J. Adelman, J. John E. Anderson, S.F. Anderson, J. Annis, N.A. Bahcall et al., *The Sloan Digital Sky Survey: Technical summary*, *AJ* **120** (2000) 1579.
- [23] E.L. Wright, P.R.M. Eisenhardt, A.K. Mainzer, M.E. Ressler, R.M. Cutri, T. Jarrett et al., *The Wide-field Infrared Survey Explorer (WISE): Mission description and initial on-orbit performance*, *AJ* **140** (2010) 1868.
- [24] P. Boubel, M. Colless, K. Said and L. Staveley-Smith, *Large-scale motions and growth rate from forward-modelling Tully–Fisher peculiar velocities*, *MNRAS* **531** (2024) 84.

- [25] E. Kourkchi, R.B. Tully, G.S. Anand, H.M. Courtois, A. Dupuy, J.D. Neill et al., *Cosmicflows-4: The calibration of optical and infrared Tully–Fisher relations*, *ApJ* **896** (2020) 3.
- [26] N. Planck Collaboration; Aghanim, Y. Akrami, M. Ashdown, J. Aumont, C. Baccigalupi, M. Ballardini et al., *Planck 2018 results - VI. cosmological parameters*, *A&A* **641** (2020) A6.
- [27] R. Trotta, *Bayes in the sky: Bayesian inference and model selection in cosmology*, *Contemporary Physics* **49** (2008) 71.
- [28] A.R. Liddle, *Statistical methods for cosmological parameter selection and estimation*, *Annual Review of Nuclear and Particle Science* **59** (2009) 95.
- [29] G. Schwarz, *Estimating the dimension of a model*, *The annals of statistics* (1978) 461.
- [30] R.E. Kass and A.E. Raftery, *Bayes factors*, *Journal of the american statistical association* **90** (1995) 773.
- [31] H. Jeffreys, *The theory of probability*, OUP Oxford (1998).
- [32] M.V. John and J. Narlikar, *Comparison of cosmological models using Bayesian theory*, *Phys. Rev. D* **65** (2002) 043506.
- [33] P.S. Drell, T.J. Loredo and I. Wasserman, *Type IA supernovae, evolution, and the cosmological constant*, *ApJ* **530** (2000) 593.
- [34] K.M. Górski, E. Hivon, A.J. Banday, B.D. Wandelt, F.K. Hansen, M. Reinecke et al., *HEALPix: A framework for high-resolution discretization and fast analysis of data distributed on the sphere*, *ApJ* **622** (2005) 759.
- [35] B.S. Koribalski, L. Staveley-Smith, T. Westmeier, P. Serra, K. Spekkens, O.I. Wong et al., *WALLABY – an SKA Pathfinder HI survey*, *ApSS* **365** (2020) .
- [36] T. Westmeier, N. Deg, K. Spekkens, T.N. Reynolds, A.X. Shen, S. Gaudet et al., *WALLABY pilot survey: Public release of H I data for almost 600 galaxies from phase 1 of ASKAP pilot observations*, *PASA* **39** (2022) e058.
- [37] J. Kang, M. Zhu, M. Ai, H. Yu and C. Sun, *Extragalactic H I Survey with FAST: First look at the pilot survey results*, *Research in Astronomy and Astrophysics* **22** (2022) 065019.
- [38] C.-P. Zhang, M. Zhu, P. Jiang, C. Cheng, J. Wang, J. Wang et al., *The FAST all sky H I survey (FASHI): The first release of catalog*, *Science China Physics, Mechanics & Astronomy* **67** (2023) .
- [39] H.M. Courtois, K. Said, J. Mould, T.H. Jarrett, D. Pomarède, T. Westmeier et al., *WALLABY pre-pilot and pilot survey: The Tully Fisher relation in Eridanus, Hydra, Norma, and NGC4636 fields*, *MNRAS* **519** (2022) 4589–4607.
- [40] C. Saulder, C. Howlett, K.A. Douglass, K. Said, S. BenZvi, S. Ahlen et al., *Target selection for the DESI Peculiar Velocity Survey*, *MNRAS* **525** (2023) 1106.
- [41] J. Carrick, S.J. Turnbull, G. Lavaux and M.J. Hudson, *Cosmological parameters from the comparison of peculiar velocities with predictions from the 2M++ density field*, *MNRAS* **450** (2015) 317.
- [42] T.P. Robitaille, E.J. Tollerud, P. Greenfield, M. Droettboom, E. Bray, T. Aldcroft et al., *Astropy: A community python package for astronomy*, *A&A* **558** (2013) A33.
- [43] A. Lewis, *Getdist: a python package for analysing monte carlo samples*, 2019.
- [44] D. Foreman-Mackey, D. Hogg, D. Lang and J. Goodman, *emcee: The MCMC hammer*, *PASP* **125** (2013) 306.
- [45] J.D. Hunter, *Matplotlib: A 2D Graphics Environment*, *Comput. Sci. Eng.* **9** (2007) 90.